Journal of Materials Chemistry C

Accepted Manuscript

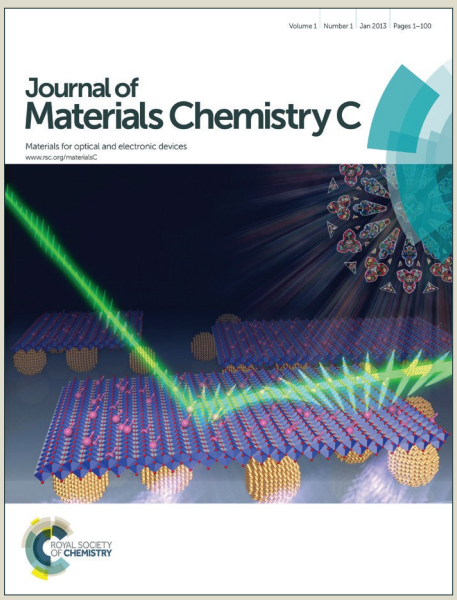

ROYAL SOCIETY OF CHEMISTRY

www.rsc.org/materialsC

Structural Evolution, Photoinduced Energy Transfer in Au Nanocluster–CdTe QD Nanocomposites and Amino Acid Sensing

Bipattaran Paramanik,[†] Sangita Kundu,[†,‡] Goutam De,[‡,*] and Amitava Patra[†,*]

[†]Department of Materials Science, Indian Association for the Cultivation of Science, Jadavpur, Kolkata 700032, India

[‡]Nano-Structured Materials Division, CSIR-Central Glass & Ceramic Research Institute, Jadavpur, Kolkata 700032, India

*Author to whom correspondence should be addressed; electronic mail: msap@iacs.res.in (Amitava Patra), Phone: (91)-33-2473-4971, Fax: (91)-33-2473-2805 and gde@cgcri.res.in (Goutam De).

Abstract

Metal-semiconductor heterostructures/composites are found to be a new class of functional materials because of their unprecedented properties and potential applications. Various strategies have been adopted to design such materials with unique properties. Here, we have synthesized Au-CdTe nanocomposites using Au nanoclusters, and the growth rate is controlled by changing Au:Cd ratio. The structural characterization of Au-CdTe nanocomposites is done by the SAXS (small angle X-ray scattering), TEM (transmission electron microscope), X-ray photoelectron spectroscopy (XPS), FTIR (Fourier transformed infrared), steady state and time resolved spectroscopy. The blue shifting of absorption band of CdTe QDs and strong photoluminescence quenching in presence of Au suggest the metal cluster-semiconductor composite formation. Time resolved spectroscopic study confirms the Förster resonance energy transfer from QDs to proximal Au nanocluster by changing of non-radiative decay rate. Interestingly, turn on of signal i.e. the enhancement of photoluminescence (PL) intensity of the nanocomposite is observed in presence of amino acid and the limit of detection (LOD) for L-cystein amino acid is found to be 192 nM. These nanocomposites open up new platforms to design optical based probes for selective sensing of amino acids.

Introduction

The metal nanoclusters (NCs) being a new class of materials having a size less than 2 nm, lies between the metal atom and nanoparticle (NP)[1-3] and these nanoclusters have various advantages like discrete electronic state, chirality, high fluorescence life time and magnetic properties due to strong quantum confinement.[1, 2, 4-8] The distinctive property of nanoclusters are intense fluorescence and molecule-like d–sp and sp–sp transitions, which are due to strong quantum confinement.[9-11] The number of atoms in the core and the capping ligands control the photoluminescence wavelength of metal nanocluster, which can be tuned from near infrared (NIR) to ultraviolet (UV).[1, 12-15] Unlike nanoparticle, the nanocluster within this size regime do not show surface plasmon resonance (SPR) because the density of state for Au NC is very low.[16-18] Therefore, due to the low density of state, molecule like single-electron transition is feasible in Au NC rather than plasmonic collective electron excitation.[19, 20]

Considering the above advantages, often Au nanoclusters are coupled with other semiconducting materials to achieve unprecedented properties. Nanocomposite of Au NC and semiconducting TiO_2 is found to be a potential candidate due to its direct application in solar cell, hydrogen generation and photocatalysis.[21] TiO_2 possess a larger band gap (3.2 eV) and acts as universal electron acceptor, but do not response in visible light.[16] Whereas, Au nanocluster can be excited under simulated solar illumination because it has size tunable band gap (1.8 and 2.8 eV).[16] Therefore the photoexcited electron injection is easily possible from Au NC to the conduction band of the TiO_2.[22] The enhanced charge separation of metal-semiconductor hetero-nanostructures is found to play crucial role on hydrogen generation, nonlinear optical as well as photocatalytic properties.[23-30] Various hybrid nanostructured architectures, including individual metal conjugated with semiconductor via a spacer,[31, 32] core/shell,[33] tetrapods,[24] and dumbbell shapes,[34] etc are reported. Generally, such heterostructures were synthesized in non-aqueous phase, mostly by surfactant mediated seed growth methods using long chain organic acids/amines.[23, 29, 35, 36] Low yield, high temperature heating, two step air sensitive reaction and costly reagents are the main drawbacks of these syntheses.[37, 38] From the application point of view, it is noted here that singlet oxygen generation is possible from Au NC-lyposome nanocomposite to kill the infectious bacteria.[39] For the detection of both Hg^{2+} and F^- ions, a single probe of Au NC-CdTe quantum dots nanocomposite is designed.[40] Previously, glutathione

capped metal nanoclusters (Au, Ag, Cu, and Pt) with tunable colors are being used for label free-detection of Hg^{2+} ion.[41] Here, our emphasis is to design Au nanocluster-QD composite and understand their photophysical properties by steady state and time resolved spectroscopy. Finally, we would like to use this optical probe for detection of amino acid which is a real challenge because amino acids are taking leading role in several biological activities.[42, 43]

Here, our emphasis is to synthesis of Au nanocluster-QDs nanocomposite by controlling the aggregation of Au NCs to develop optical sensor. In the present study, we describe an in situ method to synthesize Au NC–CdTe QDs nanocomposite by a systematic growth of Au nanocluster. The detail structural evolution of Au-CdTe system is investigated by the SAXS (small angle X-ray scattering), TEM (transmission electron microscope), X-ray photoelectron spectroscopy (XPS), FTIR (Fourier transformed infrared), steady state and time resolved spectroscopy. The fundamental photophysical studies of composition dependent metal cluster-semiconductor nanocomposite have been done by using steady state and time resolved spectroscopy. Time resolved spectroscopic study reveals that the change in nonradiative relaxation rate is due to energy transfer from QDs to Au cluster in the nanocomposite. Finally, the nanocomposites are being used as optical based sensor for probing L-cystein amino acid, selectively. It is very important to detect the amount of Cys for diagnostic purpose because the deficiency of Cys in living body causes several diseases like, depigmentation of hair, damage of liver and skin, weakness etc.[42] Above all, important biological functions like metabolism, detoxification of excess metal ions are also regulated by cystein.[44, 45]

Experimental section

Tetrachloroauric acid ($HAuCl_4$. $3H_2O$), glutathione reduced (GSH), tellurium powder and cadmium chloride hemi-pentahydrate ($CdCl_2$. 5/2 H_2O), were obtained from Sigma-Aldrich. Other chemicals like sodium borohydride ($NaBH_4$), sodium hydroxide (NaOH) and 2-propanol were received from Merck. Amino acids used for the experiment, having highest purity grade, were obtained from Spectrochem (India). Millipore deionized water (≈ 18.2 MΩ) was used for all solution preparation in this study. Dialysis tube (molecular cut off < 14 KDa) was purchased from Fischer-Chemicals. All chemicals of analytical grade were used for our experiment without further purification.

Synthesis of in situ Au NC-CdTe QDs nanocomposite

The Au NC-CdTe QDs nanocomposites were prepared by mixing the NaHTe with Cd^{2+} chelated Au-GSH complex. First, we have prepared NaHTe by following method.[40] In this typical experiment, 0.0115 g of Te powder was dispersed in 2 mL of argon saturated deionized water in a round bottom flask. The mixture was allowed to stir for 5-7 min to make uniform dispersion of Te powder. Then, 0.01 g of $NaBH_4$ was added to the mixture and vigorous stirring was continued for 30 mins and the color of the solution was changed from black to faint pink after 30 mins. Faint pink color became darker with time, suggesting the formation of fresh and highly reactive NaHTe. Argon atmosphere was maintained to preserve the highly reactive NaHTe.

Preparation of Cd^{2+} chelated gold-GSH complex:

In a round bottom flask, variable amount of chloroauric acid (0.0032 to 0.0172 g) was mixed with 0.046 g of GSH in 20 mL argon saturated water with slow stirring to get a white precipitate like Au-glutathione complex.[46] After 5 min, 1 (M) NaOH was added to adjust the pH 7.0 of the solution. The clear solution was allowed to stir for 1h to complete the Au-GSH complex formation. Then, 0.028 g of cadmium chloride hemi-pentahydrate was mixed and the pH of the solution was raised to 9.2 by adding drop by drop 1 (M) NaOH. This cadmium chelated Au-glutathione complex was left to stir for another 1 h.

Then previously prepared NaHTe was immediately injected into the Cd^{2+} chelated Au-GSH solution. This mixture solution was stirred at room temperature for another 30 min; keeping argon atmosphere. Finally the solution was heated at 110°C, argon purged situation. The Au-CdTe QDs nanocomposite having emission at 523 nm was taken out from the reaction mixture. Extensive dialysis was done to remove unreacted substances and excess capping ligand from AuNC-CdTe QDs nanocomposite. The nanocomposite solution was stored at 4^oC in dark for further use. The structure of glutathione is given in fig. S1 (see ESI†). The details of controlled experiments like synthesis of pure Au NC and CdTe QDs are given in the supporting information (see ESI†).

Fluorescence measurement of the nanocomposite with and without amino acids

QDs and the AuNC-QDs nanocomposites, having variable Au:Cd ratios were dissolved in water for fluorescence study. The samples were left to incubate at 25^0 C for overnight and the

PL of the samples was recorded. To observe the selectivity of the nanocomposites on amino acids, 20 μL of the nanocomposite solutions were used. Different types of amino acids were taken in a cuvette and the final volume of the solution was kept fixed to 3 mL. Then, the assays were incubated for overnight at 25^0 C.

Characterization

The transmission electron microscopic (TEM) image and the energy dispersive X-ray spectroscopy (EDX) were taken using JEOL-JEM-2100F transmission electron microscope. The high-angle annular dark-field imaging (HAADF) of samples are executed in scanning transmission electron microscope (STEM) mode of the same TEM instrument. X-ray photoelectron spectroscopy (XPS) measurements were carried out using an Omicron Nanotechnology instrument. Small angle X-ray scattering (SAXS) profile of all liquid samples were measured in transmission mode by Rigaku Smart Lab X-ray diffractometer (9 kW; Cu K_α radiation; λ = 1.54059 A^0). The samples were put in transparent Borosilicate capillary tube, having internal diameter almost 1.5 mm. The capillary was fixed with the sample holder and the sample alignment and premeasurement scan were carried out before run of the sample. The NANO-solver software of Rigaku was used to fit the SAXS profiles. The maximum time taken for each SAXS data acquisition was 20 min. The background correction was done in each case before fitting of the SAXS profile. Fourier transformed infrared (FTIR) spectra of the samples were recorded with Nicolet 380 FTIR by making pellet with KBr. Room-temperature optical absorption spectra were recorded by UV-VIS spectrophotometer (Shimadzu). The photoluminescence spectra of all samples were obtained with FluoroMax-P (HORIBA Jobin Yvon) luminescence spectrophotometer. All fluorescence spectra were recorded at an excitation wavelength of 375 nm at room temperature. For the time correlated single photon counting (TCSPC) measurement the samples were excited at 375 nm using a picoseconds NANO-LED IBH 375 L. The following expression was used to analyze the experimental time resolved fluorescence decays, $P(t)$;

$$P(t) = b + \sum_i^n \alpha_i \exp(-\frac{t}{\tau_i}) \quad (1)$$

Here, n is the number of emissive species and b is the baseline correction ("dc" offset), and α_i and τ_i are the pre-exponential factors and excited state fluorescence lifetimes associated with the ith component respectively. The intensity-weighted average lifetime, $<\tau>$, was calculated from the following formula

$$<\tau> = \frac{\sum_i^n a_i \tau_i^2}{\sum_i^n a_i \tau_i} \quad (2)$$

Where a_i is contribution of the decay component.

The quantum yield (QY) of all samples were obtained by comparison with reference dye, rhodamine 6G (in water), using the following equation

$$QY_s = (F_s \times A_r \times \eta_s^2 \times QY_s) / (F_r \times A_s \times \eta_r^2) \quad (3)$$

Where, F_s and F_r are the integrated fluorescence emission of the sample and the reference. A_s and A_r are the absorbance at the excitation wavelength of the sample and the reference. QY_s and QY_r are the quantum yields of the sample and the reference (QY_r = 0.95). The refractive indices of the solvents used for the preparation of the sample and reference are given by n_s (1.33) and n_r (1.33), respectively (here both solvents are water).

Results and discussion

Structural characterization

Transmission electron microscope (TEM), fourier transform infrared spectroscopy (FTIR), small angle X-ray scattering (SAXS) are being used to characterize these nanocomposite systems. Fig. 1 (A-B) shows the bright field TEM images of nanocomposite with Au:Cd ratio 0.25:1. The light contrast particles (Fig. 1A) are CdTe QDs and the dark particles are Au NCs. The dark field (HAADF) image (Fig. 1B) clearly identifies the Au nanocluster in presence of CdTe. In the dark field image of Au NCs exhibit light contrast and CdTe QDs exhibit dark contrast, unlike to the bright field image. The bright field and the dark field images confirm the presence of CdTe and Au nanocluster, suggesting in situ nanocomposite formation. Noteworthy, the TEM image of nanocomposite (Au: Cd ratio is 0.07:1) is similar (Fig. S4, ESI†) to the TEM

image of nanocomposite having Au: Cd ratio 0.25:1. In the EDX spectrum, two distinct peaks of Au and Cd (Fig. S5, ESI†) are observed which confirm the formation of Au nanocluster-CdTe QDs nanocomposites.

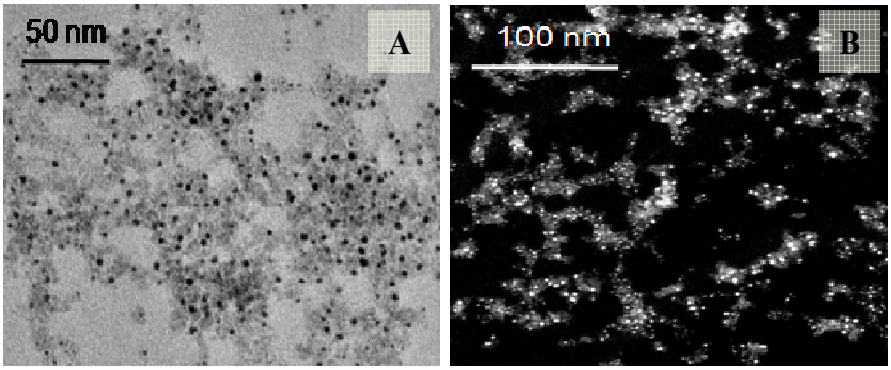

Fig. 1 Bright field TEM image (A) and HAADF image (B) of the nanocomposite, Au: Cd ratio 0.25: 1.

Small angle X-ray scattering (SAXS) is found to be important tool to evaluate size of nanocomposites.[47, 48] The working principle of SAXS is given in detail in the supporting information (ESI†).[49] Fig. S6A (ESI†) depicts both simulate and raw data of the SAXS profile of CdTe QDs in pure state. For best fitting of raw data, the only residual factor is chosen which have error value within 4 % (Fig. S6A, ESI†). The good agreement between raw and simulate data indicating the spherical model assumption is correct to analysis the SAXS data.[49] The size distribution of the CdTe QDs in pure state is shown in Fig. S6B (ESI†). The diameter of the particle (QDs) is around 2.9 nm and the narrow distribution curve indicates that the QDs are monodispersed in nature. The SAXS profile of pure Au nanoclusters (Fig. S7A, ESI†) shows that the simulate data matches well with the raw data. The size distributions of the Au NC are shown in Fig. S7B (ESI†). It is clear from the size distribution curve that the average diameter of the Au NC is 1.8 nm, very close to the TEM data. For the SAXS analysis of the nanocomposite, first we have monitored CdTe QDs and then we have monitored the Au NCs, without changing the other parameters. Background correction was done by the opposite solution to eliminate other effects. We have corrected the background by Au NCs and vice versa to find the effect of CdTe QDs in the nanocomposite. Fig. S8A (ESI†) represents SAXS profile with raw and simulated data of the

naonocomposite (Au:Cd = 0.25:1), where only CdTe is monitored. Size distributions corresponding to the CdTe QDs are given in Fig. S8B (ESI†), which is similar to pure QDs. To visualize all the SAXS profile and size distribution of CdTe, the data are given Fig. 2A and Fig. 2B, respectively. Fig. 2 and Table 1 imply that the increase of Au content does not affect the shape and size of CdTe QDs, also supported by the TEM. Noteworthy, the SAXS profile (Fig. S9A, ESI†) of Au NC in the nanocomposite (Au:Cd = 0.25:1), changes significantly with respect to the pure Au NC. It is clear from Fig. S9B (ESI†) that the size of Au NC increases from 1.8 nm to 4.0 nm. To confirm the systematic change of the size of the Au nanocluster, we have obtained the SAXS profile of the other nanocomposite (Au:Cd = 0.07:1) also. All the SAXS data of the nanocomposite (Au:Cd = 0.07:1) follows the same trend like nanocomposite (Au:Cd = 0.25:1). Therefore, the SAXS profile of the nanocomposite (Au:Cd = 0.07:1) is given in the supporting information (Fig. S10, ESI†). Interestingly, the size evolution of Au NC from 1.8 nm to 3.6 nm is also observed for 0.07:1 ratio of Au:Cd (Fig. S11, ESI†). For better representation, we have plotted all the simulated data in Fig. 3 and it reveals that a gradual increase of the size of Au nanocluster occurs. It is important to mention that we did not observe any change of size Au NC and CdTe in the physical mixture (Fig. 3, show in Table 2).

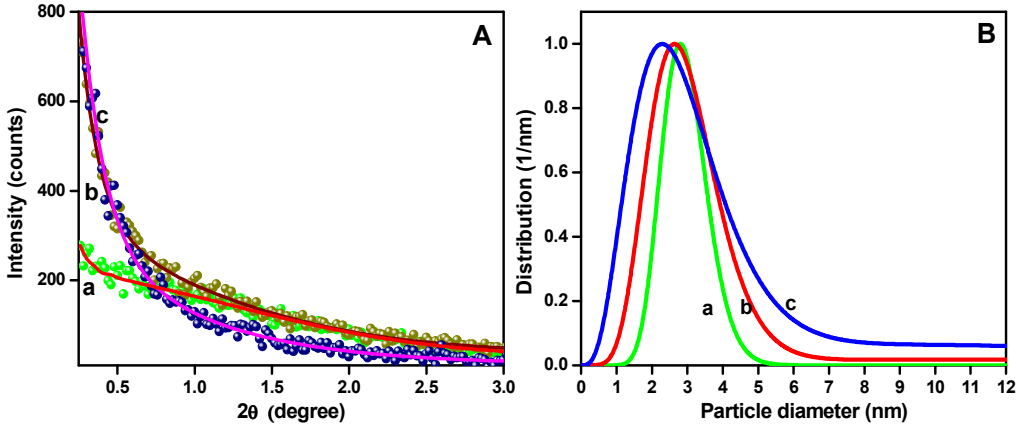

Fig. 2 SAXS profiles (A) and size distributions (B) of pure CdTe QDs (a) and nanocomposites (b and c having Au:Cd are 0.07:1 and 0.25:1, respectively); where CdTe QDs is monitored.

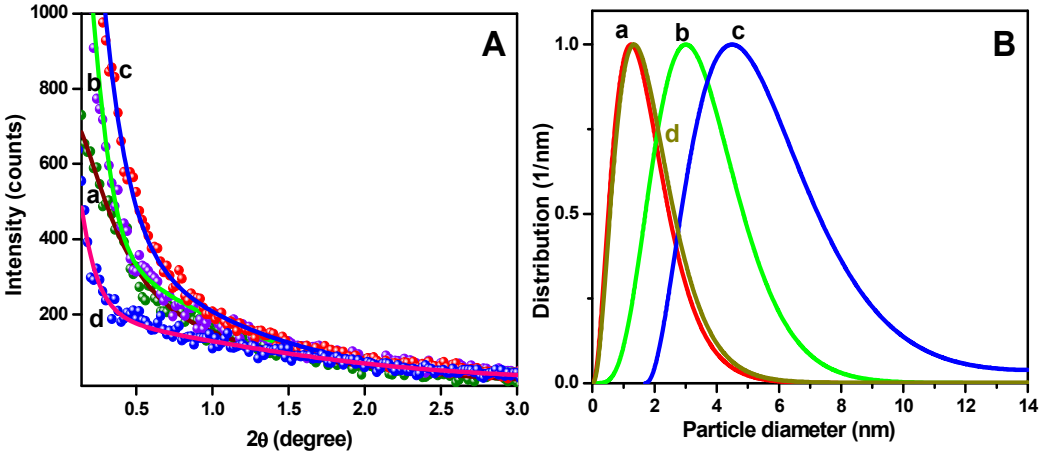

Fig. 3 SAXS profiles (A) and size distributions (B) of pure Au NC (a), nanocomposite (b and c having Au:Cd are 0.07:1 and 0.25:1, respectively) and mixture (0.07:1) (d); where AuNC is monitored.

To better characterize this nanocomposite, an XPS study was performed. In XPS study, the peaks at 405.03 eV and 411.88 eV are due to Cd $3D_{5/2}$ and $3D_{3/2}$, respectively for pure CdTe QDs (Fig. 4A), which are consistent with previous results.[50] It is seen that the binding energy of Cd $3D_{5/2}$ and $3D_{3/2}$ are shifted towards lower eV region with increasing Au:Cd ratio. The binding energy of Cd $3D_{5/2}$ and $3D_{3/2}$ are shifted to 404.57 and 411.35 eV for lower Au:Cd ratio (0.07:1). Shifting of the peaks to lower binding energy in nanocomposite system occurs due to the difference of electronegativity between atoms. The higher electronegativity of Au atom causes the shifting of Cd peak to lower eV in the present nanocomposite system.[51] Consequently, the peaks of Cd $3D_{5/2}$ and $3D_{3/2}$ are shifted to 404.02 and 410.8 eV, respectively for Au:Cd ratio (0.25:1). Thus, the systematic shifting of the Cd $3D_{5/2}$ and $3D_{3/2}$ peaks to the lower binding energy confirms the in-situ nanocomposite formation in present study. The peaks of $3D_{5/2}$ and $3D_{3/2}$ of Te for pure CdTe are appeared at 571.81 and 582.17 eV (Fig. 4B), respectively.[50] However, the $3D_{5/2}$ and $3D_{3/2}$ peaks of Te are shifted to 570.94 eV and 581.14 eV, respectively at highest Au:Cd ratio (0.25:1). Similarly, for the elements of Au in the pure Au NC, the characteristic peaks of $4f_{7/2}$ and $4f_{5/2}$ are observed at 84.23 eV and 87.93 eV (Fig. 4C), respectively.[52] Nevertheless, the $4f_{7/2}$ and $4f_{5/2}$ peaks are shifted to 83.16 eV and 87.35 eV (Fig. 4C), respectively at higher Au:Cd ratio. This spectral shifting in nanocomposites is mainly due to the interaction of the constituent (elements having different electronegativity), as depicted by the

previous reports.[51, 53, 54] In controlled experiment, the peaks for the elements Cd, Te, and Au are not shifted compare to the pure QDs and Au NC (Fig. S12, ESI†) in physical mixture (mixture of pure Au NC and QDs). This confirms the interaction of the Au NC and QDs only occur in the nanocomposite (in situ synthesis). Therefore, the systematic analysis of XPS data for the elements of Cd, Te and Au confirms the formation of nanocomposite.

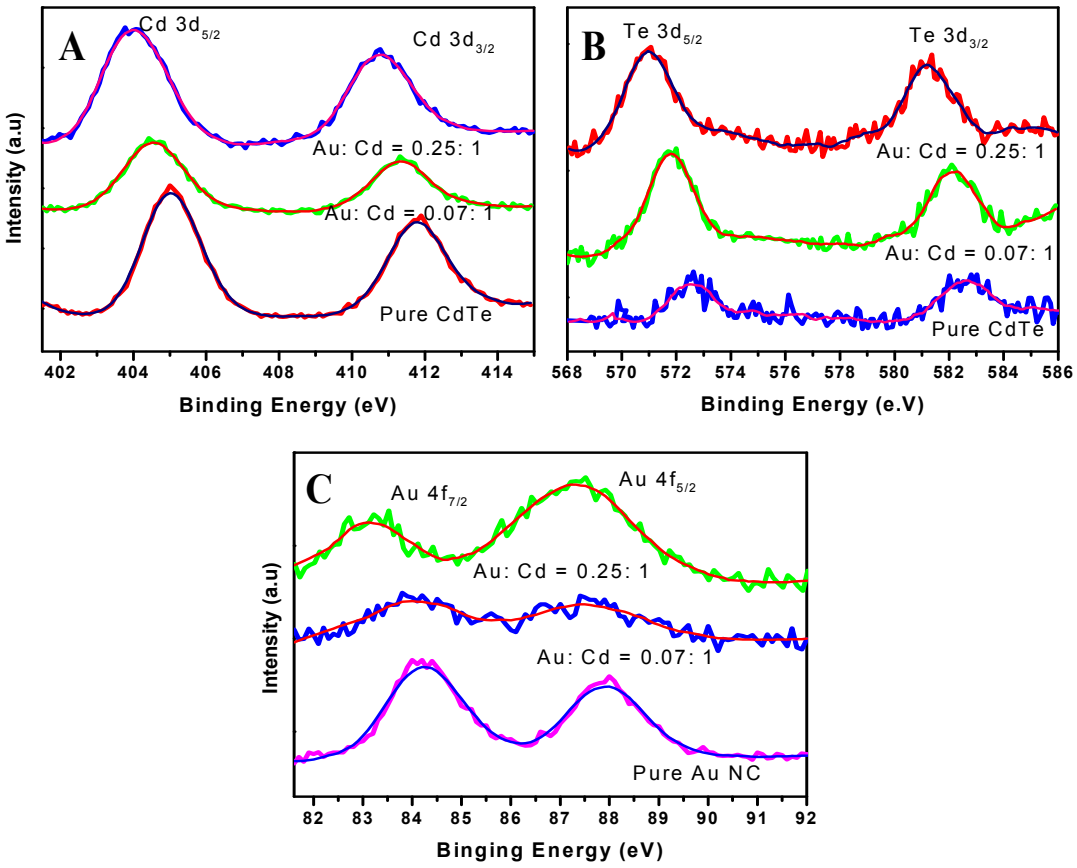

Fig. 4 XPS spectra for the elements of (A) Cd, (B) Te and (C) Au in the nanocomposite having variable of Au:Cd and in pure state.

Results from XPS, TEM and SAXS reveal that in-situ transformations formation of nanocomposites. In the FTIR spectra (Fig. S13, ESI†), the small peak at 2507 cm^{-1} is only found in the pure GSH, is responsible for the S-H stretching.[55] The absorption band at 2507 cm^{-1} is

absent in other systems, confirms the direct attachment of the S to Au NC and CdTe. The relatively strong doublet in the Au NC and CdTe at 1116 and 1074 cm^{-1} is due to the overlap of the of C-O stretching and N-C bending.[40] The doublet at 1600 cm^{-1} and 1526 cm^{-1} are responsible for carboxylate of GSH. Therefore, the FTIR spectra confirm that the both the Au NC and CdTe QDs are capped by the tripeptide GSH because of the high thiol affinity of the Au. It is well established that even Au^{3+} forms stable Au-GSH complex in presence of GSH, because of the strong thiol-gold interaction.[46] The Au-GSH complex is insoluble in water as a result precipitation occurs. The precipitate dissolves due to the de-protonation of the GSH (carboxylic acid moiety) after the addition of NaOH and the Au-GSH complexes are negatively charged after deprotonation. In solution, the negatively charged Au-GSH complexes are experienced strong repulsive interaction among themselves. This electrostatic repulsion hinders aggregation and aurophillic interaction (d^{10}-d^{10} interaction of Au) among Au-GSH complexes.[46] Therefore, Au-GSH moieties can freely move in to the solution and does not show any emission under the expose of UV torch. Chelation between the negatively charged GSH and Cd^{2+} takes place when Cd^{2+} is mixed with this solution. The chelation between Cd^{2+} and GSH become prominent (scheme 1) with time due to binding of Cd^{2+} ions with Au-GSH complex.[46, 56] In presence of Cd^{2+} ions, the aurophillic interaction between Au-GSH complexes become favorable and aggregation occurs. The Cd^{2+} bind Au-GSH complex exhibits faint orange-red emission under the exposure of UV light. Fluorescence of Au-GSH complex in presence of Cd^{2+} ions arises due to aggregation induced emission.[46] The formation of nanocomposite between CdTe and Au NC occurs after addition of Te^{2-} (NaHTe) because Cd^{2+} interacts with the highly reactive Te^{2-} (scheme 1). Therefore, Cd^{2+} takes the leading role for the in situ nanocomposite formation by controlling the aggregation of Au-GSH complex. The schematic representation of mechanism for nanocomposite formation is shown in scheme 1, which is supported experimentally in details by SAXS, XPS and FTIR.

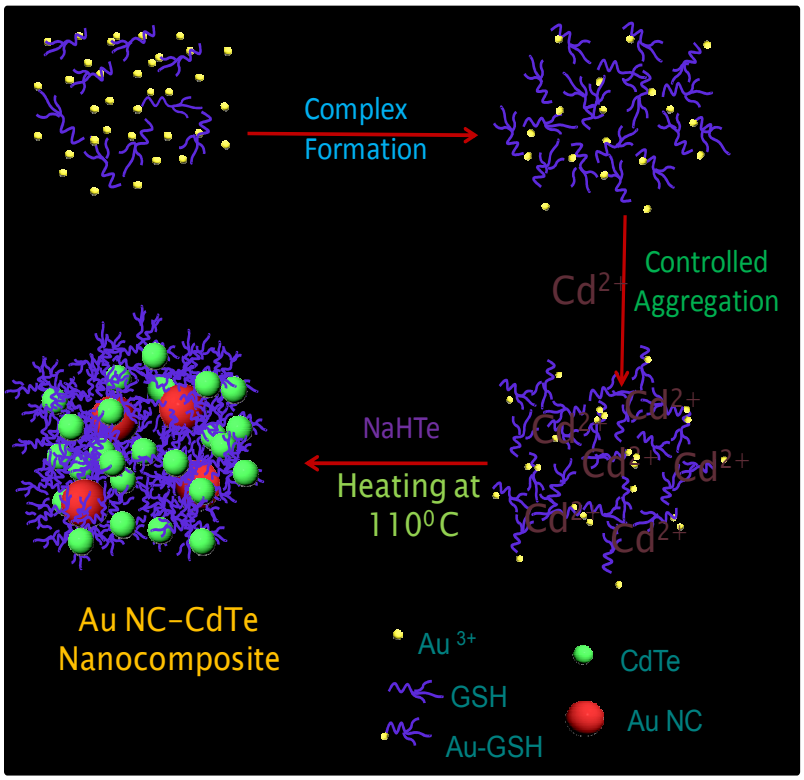

Scheme 1. Schematic representation of the Au NC-CdTe nanocomposite formation

Spectroscopic study

In Fig. 5, the strong absorption peak at 475 nm is due to the formation of pure CdTe QDs having size about 2.9 nm, which is consistent with previous results.[40] Again, we have observed that pure Au nanocluster shows a continuous absorption from 300 nm-500 nm (Fig. 5, purple line) due the sp-sp and d-sp transition of Au NC, as described by the previous reports.[2, 3, 5] However, a systematic blue shifting with enhancement of the absorbance value occurs in nanocomposite. The absorption band of QDs is shifted from 475 nm to 461 nm for the nanocomposite having Au:Cd ratio is 0.25:1 (Fig. 5). However, the physical mixture of pure CdTe QDs and Au nanocluster does not show any spectral shift. In the other nanocomposites (Au:Cd ratio 0.07:1), the blue shifting of absorption peak with respect to the pure QDs is observed and the absorption maxima of nanocomposites (Au:Cd ratio 0.07:1) is found to be at 470 nm (Fig. S14, ESI†). Therefore, the blue shifting of absorption spectra may be related to the

metal cluster-semiconductor interaction in the nanocomposite, also supported by previous report.[57]

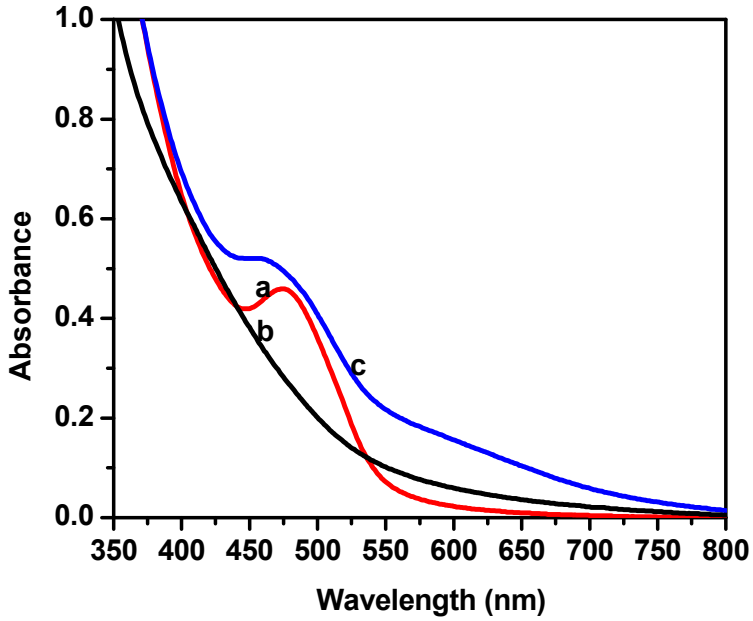

Fig. 5 The absorption spectra of pure QDs (represented by 'a' red line), pure Au NC (represented by 'b' black line) and nanocomposites (Au: Cd is 0.25:1, represented by 'c' blue line), respectively.

Fig. 6 shows the PL spectra of CdTe QDs in pure and in the nanocomposite. Pure QDs shows a strong emission at 523 nm upon the excitation at 375 nm and the emission maxima of QDs does not change in the nanocomposite. The PL intensity of QDs decreases with increasing the Au:Cd ratio. About 44% PL quenching of the QDs emission is observed in the nanocomposite having 0.07:1 ratio of Au:Cd, whereas 99 % PL quenching of the QDs is observed in the nanocomposite (Au:Cd ratio 0.25:1). There is no notable change in PL intensity in the physical mixture of pure CdTe and pure Au NC (data are not shown). We have calculated QY for pure QDs and nanocomposites (Table 3). The QY for pure CdTe is 12.0 % whereas the QY is reduced to 0.6 % for Au: Cd ratio (0.25: 1). Therefore, the dramatic decrease of PL intensity (99 %) and QY (95 %) suggests that several non-radiative processes occur in the nanocomposite, which will be discussed later in details by time resolved spectroscopy.

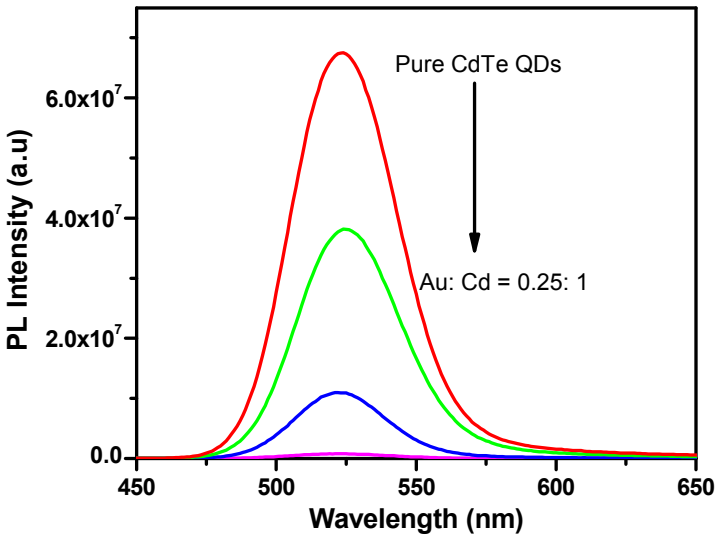

Fig. 6 The emission spectra of QDs in the nanocomposite, having variable Au:Cd ratio (0.07: 1, 0.14: 1 and 0.25: 1)

Time resolved spectroscopy is used to understand the decay dynamics of the CdTe QDs in presence of Au nanocluster in the nanocomposite (Fig. 7). The average decay time of pure QD is 29.29 ns with components of 2.24 ns (2 %), 12.5 ns (26 %) and 36.11 ns (72 %). On the other hand, the average decay time of QDs in the nanocomposite (having Au:Cd ratio is 0.07:1) is reduced to 26.42 ns, lower than the pure QDs. Corresponding decay components of nanocomposite (Au:Cd ratio is 0.07:1) are 0.67 ns (7 %), 8.59 ns (19 %) and 33.44 ns (74 %), respectively. The shortest lifetime is arising for the nanocomposite (Au:Cd ratio is 0.25:1) and it is found to be 15.30 ns. The decay components are 0.46 ns (24 %), 5.08 ns (26 %) and 27.67 ns (50 %), respectively (Table 3). The shortening of decay time of QDs is observed with increasing the Au:Cd ratio. The shortening of the decay time is reflected on the drastic change of faster component of the decay time. Though, the value of slower component of decay time is not affected significantly by the increase of Au:Cd ratio (Table 3). Noteworthy, the value of the faster component is 2.24 ns (2 %) for pure QDs and it reduces to 0.46 ns (24 %) for nanocomposite, having Au:Cd ratio is 0.25:1. The drastic change of the faster component is due to the involvement of nonradiative decay in the nanocomposite.

To find the exact fluorescence decay pathways of QDs in the nanocomposite, we have calculated the radiative and nonradiative rates (Table 3). The radiative (k_r) and nonradiative (k_{nr}) rates are calculated using the following equations;

$$k_r = \phi / \tau \quad (4)$$

and

$$k_{nr} = (1-\phi)/ \tau \quad (5)$$

ϕ and τ denotes the QY and the average lifetime of the sample, respectively. The radiative and nonradiative rates of pure QDs are 4.10×10^6 s^{-1} and 30.05×10^6 s^{-1}, respectively. The radiative and nonradiative rates in the nanocomposite (Au:Cd ratio 0.07:1) are 2.27×10^6 s^{-1} and 35.58×10^6 s^{-1}, respectively. Similarly, the radiative and nonradiative rates of the nanocomposite (Au:Cd ratio 0.25:1) are 0.39×10^6 s^{-1} and 65.13×10^6 s^{-1}, respectively. It is well established that the energy transfer is a nonradiative process, thus the drastic change in nonradiative process in the nanocomposite (having different Au:Cd ratio) is may be related to the energy transfer (ET).[31, 58]

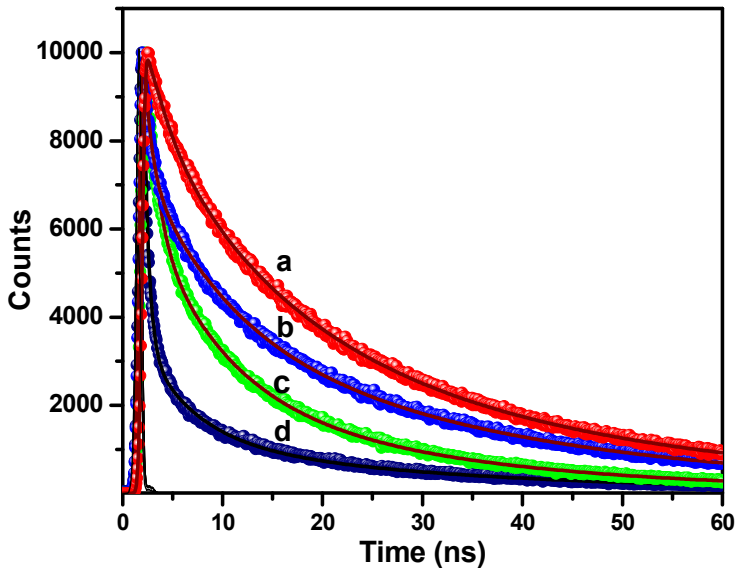

Fig. 7 The decay curves of pure CdTe QD (a) and in the nanocomposite (Au: Cd 0.07: 1, Au: Cd 0.14: 1 and Au: Cd 0.25: 1 are shown by b, c and d, respectively).

Energy transfer study

To understand the mechanism of energy transfer, the evaluation of important parameters like, spectral overlap and distance between donor and acceptor are needed. It is clearly seen that there is a good overlap between the absorption spectrum of Au NC and the emission spectrum of the CdTe QDs (Fig. S15, ESI†), indicating the possibility of energy transfer from donor QDs to the proximal Au NC in the nanocomposite.

Generally, fluorescence resonance energy transfer (FRET) involves radiationless transfer of energy from the donor fluorophore to an appropriate acceptor species. This process arises from the dipole-dipole interaction and strongly depends on the center to center distance of the donor and acceptor.[59] In the nanocluster, semiconductor like band gap arises due to the strong quantum confinement.[10] Therefore, the energy transfer from QDs to Au NC can be viewed as dipole-dipole interaction; hence the FRET model could be used, as depicted by the previous report.[58] According to the Förster theory,[60] the Förster distance is defined as the following:

$$R_0^6 = \frac{9000(\ln 10)\kappa^2\Phi_D}{128\pi^5 N n^4} J(\lambda) \quad (6)$$

where ϕ_D is the quantum yield of donor in the absence of acceptor (12.0 %), N is Avogadro's number, n is the refractive index of medium (1.33) and κ^2 is the orientation factor of two interacting dipoles. The value of κ^2 depends on the relative orientation of donor and acceptor dipoles.[59] For randomly oriented dipoles $\kappa^2 = 2/3$, and it varies between 0 and 4 for the cases of orthogonal and parallel dipoles, respectively. $J(\lambda)$ is the spectral overlap integral that is defined as the following

$$J(\lambda) = \int_0^\infty F_D(\lambda)\varepsilon_A(\lambda)\lambda^4 d\lambda \quad (7)$$

Where $F_D(\lambda)$ is the normalized emission spectrum of donor, $\varepsilon_A(\lambda)$ is the absorption coefficient of acceptor at wavelength λ (in nm). Again, according to the Förster theory the rate of the energy transfer for donor-acceptor pair separated by a distance 'r' is given by the following equation:

$$k_T(r) = \frac{1}{\tau_D}\left(\frac{R_0}{r}\right)^6 \quad (8)$$

where $k_T(r)$ and τ_D are the rate of the energy transfer and lifetime of the donor in absence of the acceptor, respectively. Noteworthy, the spectral overlap between donor QDs and the acceptor Au NC increases with increasing the Au:Cd ratio in the nanocomposite. The calculated overlap integrals are found to be 2.24 $\times 10^{15}$, 2.41 $\times$ 10^{15} and 2.73 $\times$ 10^{15} M^{-1} cm^{-1} nm^4, for the nanocomposite systems (having Au:Cd are 0.007:1, 0.14:1 and 0.25:1), respectively. Förster distances between the donor and acceptor are found to be 38.72, 39.20 and 40.58 Å for the nanocomposite (having Au:Cd are 0.007:1, 0.14:1 and 0.25:1), respectively. We have calculated the donor-acceptor distance and rate of energy transfer using FRET model. The distance between donor and acceptor for nanocomposite (Au:Cd ratio is 0:007:1) is found to be 56.05 Å and the distance is decreased to 43.25 Å for the nanocomposite having 0.14:1 ratio of Au: Cd ratio. However, the shortest donor-acceptor appears in the nanocomposite having Au: Cd is 0.25:1 and the estimated donor-acceptor distance is 40.58 Å. The rate of energy transfer in the nanocomposite is also affected by the change of the donor-acceptor distance. The donor-acceptor distance decreases with increasing the Au:Cd ratio in the nanocomposite, therefore the rate of energy transfer is increased. The rate of energy transfer is found to be 3.71 $\times$ 10^6 s^{-1}, 18.90 $\times$ 10^6 s^{-1} and 31.41 $\times$ 10^6 s^{-1} for the nanocomposite, Au:Cd ratios are 0.007:1, 0.14:1 and 0.25:1, respectively. We have also calculated the energy transfer efficiency is by using the following equation,

$$\phi_{ET} = 1 - (\tau_{DA}/\tau_D) \quad (9)$$

where, ϕ_{ET}, τ_{DA} and τ_D are the energy transfer efficiency, decay time of QDs in nanocomposite and in pure state, respectively. The obtained energy transfer efficiency (Table 3) changes from 9.8 % to 35.6 % with changing the Au:Cd ratio from 0.07: 1 to 0.14:1. However, the highest energy transfer efficiency is obtained in the nanocomposite (Au:Cd ratio 0.25: 1) and it is found to be 47.9 %. Therefore, the increase of energy transfer efficiency with increasing the Au content in the nanocomposite is not only due to the better spectral overlap between the donor-acceptor but also due to the close proximity of the acceptor Au nanocluster around the QDs surface.

Sensing of amino acid

These metal cluster-semiconductor nanocomposites (Au: Cd ratio 0.07:1) are being used as optical based sensor for probing different amino acids. Fig. 8 shows the drastical increment in PL intensity of the nanocomposite with the addition of the L-Cys amino acid. Other amino acids do not exhibit significant change in the PL intensity, the concentration of other amino acids was taken 10 times higher than the L-Cys. Analysis of the histogram (Fig. 9) reveals that this nanocomposite is very selective to L-Cys. The PL intensity of the nanocomposite does not show any enhancement even in the mixture of all amino acids (except L-Cys). However, about 55% enhancement of the PL intensity of this nanocomposite is observed in presence of L-Cys which confirms high sensitivity and selectivity of the nanocomposite to the L-Cys. In the controlled experiment, we have observed that pure CdTe QDs does not show any PL enhancement in presence of L-Cys. The enhancement of PL intensity of the nanocomposite in presence of L-Cys, is said to be turn on of the signal. Thus, this nanocomposite could be used as a turn on optical probe for the sensing of L-Cys.

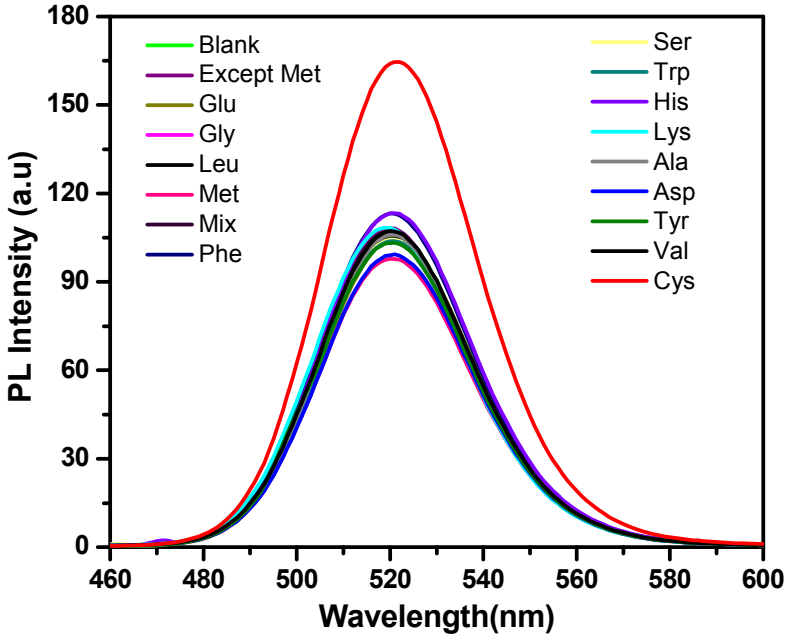

Fig. 8 The PL response of the composite probe in presence of different amino acids

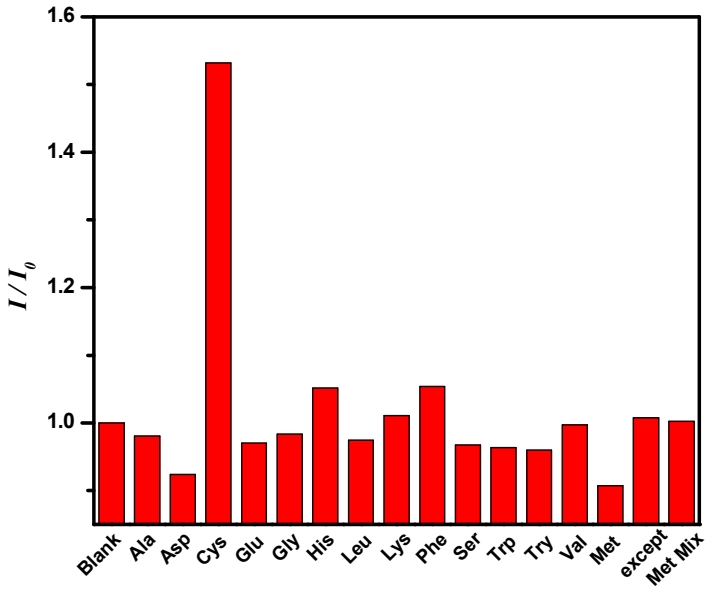

Fig. 9 Histogram of the PL intensity of the composite probe in presence of different amino acids.

Fig. 10A demonstrates the enhancement of PL intensity in presence of variable concentration of L-Cys. The maximum enhancement of PL intensity is observed for the 24.6 μM concentration of L-Cys, after that saturation occurs. To get the calibration curve, the enhanced PL intensity of the nanocomposite is plotted against the concentration of L-Cys (Fig. 10B). The probe shows a very good linear behavior up to 24.6 μM concentration of L-Cys. The limit of detection (LOD) for L-Cys is calculated from the slope and the intercept of the calibration line and the LOD for L-Cys is found to be 192 nM in the present study. Therefore, this nanocomposite system could be used as an optical sensor for the detection of L-Cys, using turn on approach.

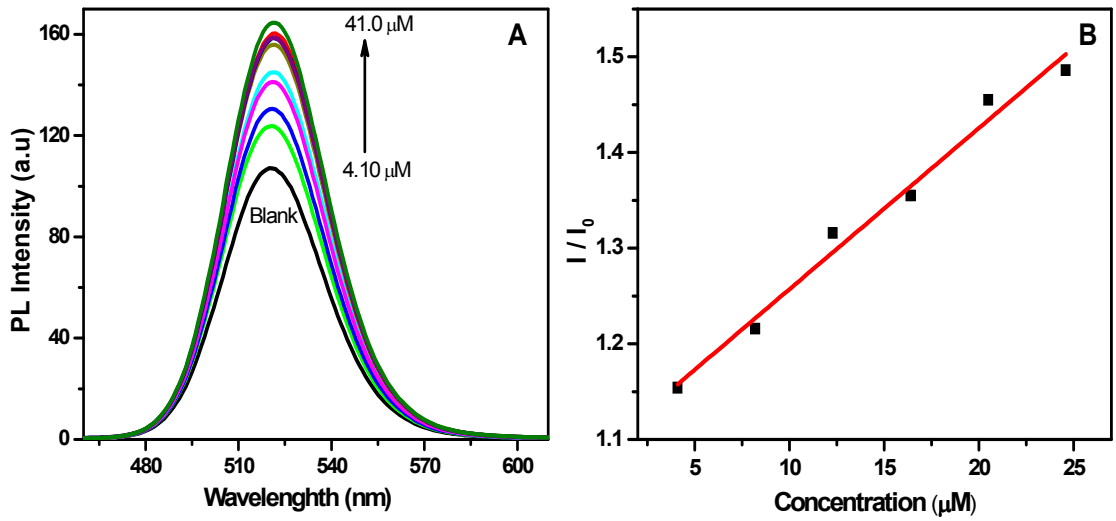

Fig. 10 The enhancement of PL intensity of the nanocomposite probe (Au:Cd is 0.07: 1) in presence of different concentrations of L-Cys (A). The calibration curve of L-Cys to calculate the limit of detection (LOD) (B).

The nanocomposites with the ratio of Au:Cd is 0.14:1 could also be used for the detection of L-Cys. It is clear from Fig. S16A (ESI†) that the PL enhancement of the nanocomposite (having Au:Cd is 0.14: 1) occurs in presence of L-Cys. However, the PL enhancement of this nanocomposite is much lower than the nanocomposites (Au:Cd is 0.07: 1) for same L-Cys concentration. The LOD is found to be 268 nM for the nanocomposite (having Au:Cd is 0.14: 1) from Fig. S16B (ESI†), which is much higher than LOD value in nanocomposite (Au:Cd is 0.07: 1). Lower efficiency of the nanocomposite (Au:Cd is 0.14: 1) is due to the lower QY than the nanocomposite (having Au:Cd is 0.07: 1, Table 3).

The plausible mechanism for PL enhancement of the nanocomposite in presence of L-Cys is proposed. L-Cysteine contains thiol (SH) group. Thiols have very strong affinity to the Au or Ag metals due to the soft-soft interactions.[46] Generally, if thiol containing ligands are incubated with the Au NC, sulfur group interacts with the Au NC and form Au-S bond. However, L-Cys can interact with different way with the nanocluster. It is suggested.[43, 61] that the etching of the GSH capped nanocluster is observed in presence of L-Cys due to the small size of L-Cys. To support the hypothesis, we have performed XPS and lifetime measurement of the nanocomposite (Au:Cd is 0.07: 1) in absence and presence of L-Cys. The XPS spectra (Fig.

S17A, ESI†) for Au (in the nanocomposite) in presence of L-Cys is found to be at 84.12 and 87.81 eV for $4f_{7/2}$ and $4f_{5/2}$, respectively, which is similar to the nanocomposite in absence of L-Cys (Fig. 4C). However, the XPS of the S (in the nanocomposite) changes significantly in presence of L-Cys. In absence of L-Cys, Fig. S17B (ESI†) depicts that the spectrum of S is highly symmetric in nature (peak maxima is at 161.96 eV). Nevertheless, the spectrum became asymmetric due to arise of a new peak at the higher binding energy (at around 163.0 eV) in presence of L-Cys. The peak at 161.96 eV (Fig. S17B, ESI†, both in presence and absence of L-Cys) is due to the Au bound S in the nanocluster, which is consistent with previous report.[62] The curve is deconvoluted (Fig. S17C, ESI†) to analysis the asymmetric nature of the S peak in presence of L-Cys,. The deconvoluted spectrum suggests that the new peak arises at 163.07 eV (Fig. S17C, ESI†) which is due to S-S bond formation.[14, 62] The S-S bond formation is further supported by the FTIR spectra of the nanocomposite in presence of L-Cys (Fig. S18, ESI†). A very weak peak close to 587 cm^{-1} is observed in the nanocomposite only in presence of L-Cys, due to the S-S bond formation, as suggested by the previous report.[63] However, the peak is absent in pure L-Cys and nanocomposite (in absence of L-Cys). Noteworthy, we have incubated the nanocomposite only with L-Cys, which only has S-H group, thus in-situ S-S bond is formed after the incubation. It is well established that the S-S bond is formed during etching and the deconvoluted XPS the spectra (Fig. S17C, ESI†) suggest that S-S bond formation.[64] Therefore the PL enhancement of the nanocomposite in presence of L-Cys could be due to the etching of the Au NC in the nanocomposite. However, the other possibility is the displacement of GSH by L-Cys may. To confirm the inhibition of energy transfer from QDs to Au NC, after the incubation of L-Cys, we have performed the time resolved measurement. Fig. S19 (ESI†) depicts the lifetime of the nanocomposite increases in presence of L-Cys in compare to the nanocomposite in absence of L-Cys. The average lifetime of the nanocomposite in presence of L-Cys is found to be 28.34 ns whereas it was 26.24 ns (Table 3) in absence of L-Cys. The decay components of the nanocomposite in presence of L-Cys are found to be 1.02 (2 %), 8.52 (18 %) and 33.48 ns (80 %). Therefore, the enhancement of lifetime in presence of L-Cys confirms the restriction of ET from donor QDs to Au NC quencher. Possibly etching of the Au NC (quencher) by L-Cys is the main reason behind the turn on (PL enhancement) of the nanocomposite.

Conclusion

In summary, Au nanocluster-CdTe QDs nanocomposites are synthesized from Au clusters and photophysical properties of metal-semiconductor nanocomposites are found to be composition dependent. The blue shifting of absorption band of QDs and photoluminescence quenching is related to metal cluster-semiconductor interactions in the nanocomposite. Time resolved spectroscopic study confirms the Förster resonance energy transfer process from QDs to Au cluster under photoexcitation. Furthermore, the energy transfer process from QDs to Au cluster is stalled due to the strong Au-S interaction in presence of L-Cys, as a result turn on of the PL signal is observed. The PL signal enhancement has been used to detect the L-Cys amino acid selectively and the LOD for L-Cys is found to be 192 nM. Thus, we may conclude that this new optical probe of Au NC-QD nanocomposites would be very promising for detection of amino acids.

Acknowledgement

"DAE-SRC Outstanding Investigator Award" is gratefully acknowledged for financial support. BP thanks CSIR for awarding fellowship. SK thanks DST-INSPIRE for her fellowship.

† **Electronic Supplementary Information (ESI) available:** Experimental details of pure Au NC and CdTe QDs; working principle of SAXS; TEM image of pure Au NC, pure CdTe and nanocomposite; EDX of nanocomposite; SAXS profile and size distribution of nanocomposite; XPS spectra of the physical mixture; FTIR spectra; absorption spectra of Au NC,CdTe QDs and nanocomposites; spectral overlap between CdTe QDs and Au NC; PL enhancement and LOD of the nanocomposite in presence of L-Cys; XPS and FTIR spectra of nanocomposite in presence of L-Cys; decay curves of the nanocomposite in presence and absence of L-Cys. See DOI: 10.1039/

References:

1 J. Zheng, P. R. Nicovich and R. M. Dickson, *Annu. Rev. Phys. Chem.*, 2007, **58**, 409-431.

2 R. Jin, *Nanoscale*, 2010, **2**, 343-362.

3 J. Zheng, C. Zhang and R. M. Dickson, *Phys. Rev. Lett.*, 2004, **93**, 077402.

4 M.-C. Daniel and D. Astruc, *Chem. Rev.*, 2004, **104**, 293-346.

5 H. Qian, M. Zhu, Z. Wu and R. Jin, *Acc. Chem. Res.*, 2012, **45**, 1470-1479.

6 R. Jin, *Nanoscale*, 2015, **7**, 1549-1565.

7 R. Jin, S.-K. Eah and Y. Pei, *Nanoscale*, 2012, **4**, 4026-4026.

8 E. Sharon, N. Enkin, H. B. Albada and I. Willner, *Chem. Commun.*, 2015, **51**, 1100-1103.

9 L. Shang, S. Brandholt, F. Stockmar, V. Trouillet, M. Bruns and G. U. Nienhaus, *Small*, 2012, **8**, 661-665.

10 M. Zhu, C. M. Aikens, F. J. Hollander, G. C. Schatz and R. Jin, *J. Am. Chem. Soc.*, 2008, **130**, 5883-5885.

1 Y. Zhu, H. Qian and R. Jin, *J. Mater. Chem.*, 2011, **21**, 6793-6799.

12 Z. Wu and R. Jin, *Nano Lett.*, 2010, **10**, 2568-2573.

13 B. Liao, J. Chen, H. Huang, X. Li and B. He, *J. Mater. Chem.*, 2011, **21**, 5867-5869.

14 B. Paramanik and A. Patra, *J. Mater. Chem. C*, 2014, **2**, 3005-3012.

15 J. Sun, J. Zhang and Y. Jin, *J. Mater. Chem. C*, 2013, **1**, 138-143.

16 C. Yu, G. Li, S. Kumar, H. Kawasaki and R. Jin, *J. Phys. Chem. Lett.*, 2013, **4**, 2847-2852.

17 B. Varnholt, R. Letrun, J. J. Bergkamp, Y. Fu, O. Yushchenko, S. Decurtins, E. Vauthey, S.-X. Liu and T. Burgi, *Phys. Chem. Chem. Phys.*, 2015, **17**, 14788-14795.

18 A. Arbouet, C. Voisin, D. Christofilos, P. Langot, N. D. Fatti, F. Vallée, J. Lermé, G. Celep, E. Cottancin, M. Gaudry, M. Pellarin, M. Broyer, M. Maillard, M. P. Pileni and M. Treguer, *Phys. Rev. Lett.*, 2003, **90**, 177401.

19 K.-S. Lee and M. A. El-Sayed, *J. Phys. Chem. B*, 2006, **110**, 19220-19225.

20 C. M. Hofmann, J. B. Essner, G. A. Baker and S. N. Baker, *Nanoscale*, 2014, **6**, 5425-5431.

21 Y.-S. Chen, H. Choi and P. V. Kamat, *J. Am. Chem. Soc.*, 2013, **135**, 8822-8825.

22 Y.-S. Chen and P. V. Kamat, *J. Am. Chem. Soc.*, 2014, **136**, 6075-6082.

23 R. Costi, A. E. Saunders, E. Elmalem, A. Salant and U. Banin, *Nano Lett.*, 2008, **8**, 637-641.

24 K. T. Yong, Y. Sahoo, M. T. Swihart and P. N. Prasad, *Adv. Mater.*, 2006, **18**, 1978-1982.

25 M. Lunz, V. A. Gerard, Y. K. Gun'ko, V. Lesnyak, N. Gaponik, A. S. Susha, A. L. Rogach and A. L. Bradley, *Nano Lett.*, 2011, **11**, 3341-3345.

26 M. J. Berr, A. Vaneski, C. Mauser, S. Fischbach, A. S. Susha, A. L. Rogach, F. Jäckel and J. Feldmann, *Small*, 2012, **8**, 291-297.

27 V. Sreeramulu, K. K. Haldar, A. Patra and D. N. Rao, *J. Phys. Chem. C*, 2014, **118**, 30333-30341.

28 N. Razgoniaeva, S. Lambright, N. Sharma, A. Acharya, E. Khon, P. Moroz, A. Razgoniaev, A. Ostrowski and M. Zamkov, *J. Phys. Chem. C*, 2015, **119**, 15562-15571.

29 A. Figuerola, M. v. Huis, M. Zanella, A. Genovese, S. Marras, A. Falqui, H. W. Zandbergen, R. Cingolani and L. Manna, *Nano Lett.*, 2010, **10**, 3028-3036.

30 K. K. Haldar, G. Sinha, J. Lahtinen and A. Patra, *ACS Appl. Mater. Interfaces*, 2012, **4**, 6266-6272.

31 T. Pons, I. L. Medintz, K. E. Sapsford, S. Higashiya, A. F. Grimes, D. S. English and H. Mattoussi, *Nano Lett.*, 2007, **7**, 3157-3164.

32 K. K. Haldar, T. Sen, S. Mandal and A. Patra, *ChemPhysChem*, 2012, **13**, 3989-3996.

33 J. Zhang, Y. Tang, K. Lee and M. Ouyang, *Science*, 2010, **327**, 1634-1638.

34 T. Mokari, E. Rothenberg, I. Popov, R. Costi and U. Banin, *Science*, 2004, **304**, 1787-1790.

35 K. K. Haldar, N. Pradhan and A. Patra, *Small*, 2013, **9**, 3424-3432.

36 J. Yang, E. Sargent, S. Kelley and J. Y. Ying, *Nat. Mater.*, 2009, **8**, 683-689.

37 Y.-b. Lee, S. Park, S. Lee, J. Kim, K.-S. Lee and J. Joo, *J. Mater. Chem. C*, 2013, **1**, 2145-2151.

38 Y. Lou, Y. Zhao, J. Chen and J.-J. Zhu, *J. Mater. Chem. C*, 2014, **2**, 595-613.

39 W.-Y. Chen, L.-Y. Chen, C.-M. Ou, C.-C. Huang, S.-C. Wei and H.-T. Chang, *Anal. Chem.*, 2013, **85**, 8834-8840.

40 B. Paramanik, S. Bhattacharyya and A. Patra, *Chem. Euro. J.*, 2013, **19**, 5980-5987.

41 X. Yuan, Z. Luo, Q. Zhang, X. Zhang, Y. Zheng, J. Y. Lee and J. Xie, *ACS Nano*, 2011, **5**, 8800-8808.

42 E. Weerapana, C. Wang, G. M. Simon, F. Richter, S. Khare, M. B. D. Dillon, D. A. Bachovchin, K. Mowen, D. Baker and B. F. Cravatt, *Nature*, 2010, **468**, 790-795.

43 X. Yuan, Y. Tay, X. Dou, Z. Luo, D. T. Leong and J. Xie, *Anal. Chem.*, 2013, **85**, 1913-1919.

44 K. G. Reddie and K. S. Carroll, *Curr. Opin. Chem. Biol.*, 2008, **12**, 746-754.

45 R. O. Ball, G. Courtney-Martin and P. B. Pencharz, *J. Nutr.*, 2006, **136**, 1682S-1693S.

46 Z. Luo, X. Yuan, Y. Yu, Q. Zhang, D. T. Leong, J. Y. Lee and J. Xie, *J. Am. Chem. Soc.*, 2012, **134**, 16662-16670.

47 Y. Zhang, F. Lu, K. G. Yager, D. van der Lelie and O. Gang, *Nat. Nano*, 2013, **8**, 865-872.

48 S. Manet, A. Lecchi, M. Impéror-Clerc, V. Zholobenko, D. Durand, C. L. P. Oliveira, J. S. Pedersen, I. Grillo, F. Meneau and C. Rochas, *J. Phys. Chem. B*, 2011, **115**, 11318-11329.

49 A. Baksi, A. Mitra, J. S. Mohanty, H. Lee, G. De and T. Pradeep, *J. Phys. Chem. C*, 2015, **119**, 2148-2157.

50 F. Aldeek, L. Balan, G. Medjahdi, T. Roques-Carmes, J.-P. Malval, C. Mustin, J. Ghanbaja and R. Schneider, *J. Phys. Chem. C*, 2009, **113**, 19458-19467.

51 D. R. Kauffman, D. Alfonso, C. Matranga, H. Qian and R. Jin, *J. Phys. Chem. C*, 2013, **117**, 7914-7923.

52 T. Udayabhaskararao, Y. Sun, N. Goswami, S. K. Pal, K. Balasubramanian and T. Pradeep, *Angew. Chem., Int. Ed.*, 2012, **51**, 2155-2159.

53 L. Ye, J. Fu, Z. Xu, R. Yuan and Z. Li, *ACS Appl. Mater. Interfaces*, 2014, **6**, 3483-3490.

54 R. Huang, H. Ge, X. Lin, Y. Guo, R. Yuan, X. Fu and Z. Li, *RSC Adv.*, 2013, **3**, 1235-1242.

55 M. A. H. Muhammed, P. K. Verma, S. K. Pal, R. C. A. Kumar, S. Paul, R. V. Omkumar and T. Pradeep, *Chem. Euro. J*, 2009, **15**, 10110-10120.

56 V. Lesnyak, A. Wolf, A. Dubavik, L. Borchardt, S. V. Voitekhovich, N. Gaponik, S. Kaskel and A. Eychmüller, *J. Am. Chem. Soc.*, 2011, **133**, 13413-13420.

57 E. Shaviv, O. Schubert, M. Alves-Santos, G. Goldoni, R. Di Felice, F. Vallée, N. Del Fatti, U. Banin and C. Sönnichsen, *ACS Nano*, 2011, **5**, 4712-4719.

58 F. Aldeek, X. Ji and H. Mattoussi, *J. Phys. Chem. C*, 2013, **117**, 15429-15437.

59 Joseph R. Lakowicz, *Principles of fluorescence spectroscopy, 3rd Ed.,* Springer, New York, 2006.

60 T. Forster, *Discuss. Faraday Soc.*, 1959, **27**, 7-17.

61 T. Shu, L. Su, J. Wang, C. Li and X. Zhang, *Biosens. Bioelectron.*, 2015, **66**, 155-161.

62 M.-X. Zhang, R. Cui, Z.-Q. Tian, Z.-L. Zhang and D.-W. Pang, *Adv. Funct. Mater.*, 2010, **20**, 3673-3677.

63 J. Zhang, Y. Li, J. Li, Z. Zhao, X. Liu, Z. Li, Y. Han, J. Hu and A. Chen, *Powder Technol.*, 2013, **246**, 356-362.

64 Y. Yu, Q. Yao, Z. Luo, X. Yuan, J. Y. Lee and J. Xie, *Nanoscale*, 2013, **5**, 4606-4620.

Table 1. The particle size distributions of pure CdTe and nanocomposites

Sample	Particle size (nm)	Normalized Distribution (%)	Volume (%)	R factor (%)
Pure QD	2.9	21.8	92.17	2.24
Nanocomposite (Au:CdTe =0.07:1)	2.9	33.8	84.94	1.98
Nanocomposite (Au:CdTe =0.14:1)	2.9	46.9	74.05	5.43
Mixture	2.9	31.5	96.33	2.56

Table 2. The particle size distributions of Au naocluster and nanocomposites

Sample	Particle size (nm)	Normalized Distribution (%)	Volume (%)	R factor (%)
Pure AuNC	1.8	29.0	86.71	3.28
Nanocomposite (Au: CdT =0.07:1)	3.6	40.4	87.19	2.23
Nanocomposite (Au: CdTe =0.14:1)	4.0	55.0	85.70	2.30
Mixture	1.9	54.0	97.85	2.71

Table 3. The Average decay times, quantum yields, radiative rates, nonradiative rates and energy transfer efficiencies of pure CdTe QDs and nanocomposites

Au: Cd ratio	Emission (nm)	τ_1 in ns (a_1)	τ_2 in ns (a_2)	τ_3 in ns (a_3)	$<\tau>$ (ns)	QY (%)	$K_r \times 10^6$ (s^{-1})	$K_{nr} \times 10^6$ (s^{-1})	ϕ_{ET} (%)
0	523	2.24 (0.02)	12.5 (0.26)	36.11 (0.72)	29.29	12.0	4.10	30.05	---
0.07:1	523	0.67 (0.07)	8.59 (0.19)	33.44 (0.74)	26.24	6.0	2.27	35.58	9.8
0.14:1	523	1.03 (0.12)	7.52 (0.26)	27.10 (0.62)	18.85	5.0	2.65	50.39	35.6
0.25:1	523	0.46 (0.24)	5.08 (0.26)	27.67 (0.50)	15.26	0.6	0.39	65.93	47.9

TOC: Photoluminescence quenching and enhancement of the Au NC-CdTe nanocomposite.